Icarus 221 (2012) 508–516

Contents lists available at SciVerse ScienceDirect

Icarus

journal homepage: www.elsevier.com/locate/icarus

Diurnal variation of electron density in Saturn's ionosphere: Model comparisons with Saturn Electrostatic Discharge (SED) observations

Luke Moore [a,*], Georg Fischer [b,c], Ingo Müller-Wodarg [a,d], Marina Galand [a,d], Michael Mendillo [a]

[a] Center for Space Physics, Boston University, Boston, MA 02215, USA
[b] Space Research Institute, Austrian Academy of Sciences, Graz, Austria
[c] Department of Physics and Astronomy, University of Iowa, Iowa City, IA 52242, USA
[d] Space and Atmospheric Physics Group, Department of Physics, Imperial College London, London, UK

ARTICLE INFO

Article history:
Received 20 April 2012
Revised 11 July 2012
Accepted 13 August 2012
Available online 30 August 2012

Keywords:
Aeronomy
Ionospheres
Lightning
Saturn

ABSTRACT

Using the Saturn Thermosphere Ionosphere Model (STIM), we present a study of the diurnal variation of electron density, with a focus on comparisons with peak electron densities (N_{MAX}) inferred from the low-frequency cutoff of radio emission due to lightning in the lower atmosphere, called Saturn Electrostatic Discharges (SEDs). It is demonstrated that photochemistry in Saturn's ionosphere cannot reproduce the SED-inferred diurnal variation in N_{MAX} unless additional production and loss sources outside of the current best estimates are considered. Additional explanations of the SED-inferred diurnal variation of N_{MAX} are presented and analyzed, such as the possibility that the low-frequency cutoff seen in SEDs is due to the presence of sharp low-altitude layers of plasma, as frequently seen in radio occultation measurements. Finally, we outline the observational constraints that must be fulfilled by any candidate explanations of the SED-inferred diurnal variation of N_{MAX}.

1. Introduction

1.1. SED detection history

During the 12 November 1980 Voyager 1 encounter with Saturn, the Planetary Radio Astronomy (PRA) instrument detected mysterious, broadband, short-lived, impulsive radio emission, termed Saturn Electrostatic Discharges (SEDs) (Warwick et al., 1981). SED emission was present below 100 kHz, meaning that any intervening ionosphere would have to have an electron density less than ~100 cm^{-3}, counter to the ~10^4 cm^{-3} value measured by the radio science team (Tyler et al., 1981). This fact, combined with the ~10 h periodicity of the SEDs, led Warwick et al. to conclude that they most likely originated in Saturn's rings, a claim seemingly reinforced by the detection of a new feature in Saturn's B ring by Voyager 2 (Evans et al., 1982). Burns et al. (1983), however, argued for an atmospheric source for SEDs, owing primarily to their similarity with other planetary lightning emission. They noted that shadowing by Saturn's rings would reduce the local equatorial electron density, thereby providing a possible explanation of the detection of unusually low frequency SEDs. Kaiser et al. (1983) supported the case for an atmospheric SED source by demonstrating that a ring source should have led to a longer SED detection window than was observed.

The Radio and Plasma Wave Science (RPWS) instrument aboard Cassini began detecting SEDs prior to its orbital insertion on 1 July 2004, and has since observed nine distinct storm periods, separated by quiet periods (with no SED activity) of a few days to 21 months (Fischer et al., 2011a). Shortly after Cassini's arrival at Saturn the Imaging Science Subsystem instrument detected a large storm system at 35°S planetocentric latitude that correlated with the SED recurrence pattern (Porco et al., 2005). Dyudina et al. (2007) extended this finding by presenting three further storm systems where SED observations were correlated with the rising and setting of a visible storm on the Saturn radio horizon. Finally, lightning flashes were imaged directly by Cassini in 2009, providing a convincing demonstration that SEDs were indeed signatures of storms in Saturn's atmosphere (Dyudina et al., 2010).

1.2. SED characteristics and ionospheric implications

SEDs have a large frequency bandwidth, but appear as narrow-banded streaks in both Voyager PRA and Cassini RPWS dynamic spectra, due to the short duration of the radio burst and the frequency sampling nature of the receivers. SED burst durations are typically <0.5 s, with e-folding times ranging from ~37 to 49 ms (Zarka and Pedersen, 1983; Fischer et al., 2007, 2008). The number of SEDs detected in an individual storm varies dramatically, from hundreds to tens of thousands (Fischer et al., 2008), with typical burst rates of a few hundred per hour (Zarka and Pedersen, 1983; Fischer et al., 2006). SED *storms* are periods of nearly

* Corresponding author.
E-mail address: moore@bu.edu (L. Moore).

0019-1035/$ - see front matter © 2012 Elsevier Inc. All rights reserved.
http://dx.doi.org/10.1016/j.icarus.2012.08.010

continuous SED activity, modulated by *episodes* of varying SED activity. The recurrence period of the episodes within a storm represents the time between peaks of SED activity; for a single longitudinally confined storm system, therefore, this period is related to the rotation rate of the atmosphere. Recurrence periods for Voyager 1 and Voyager 2 SEDs episodes were ~10 h 10 min and ~10 h 00 min, respectively (Evans et al., 1981; Warwick et al., 1982), and were therefore thought to originate from equatorial storm systems (Burns et al., 1983), though none were observed directly. In contrast, aside from one weak storm in June 2005, all recurrence periods for the Cassini era SED storms are near 10 h 40 min (Fischer et al., 2008), implying a mid-latitude origin, as confirmed by the 35°S latitude clouds and visible lightning flashes imaged by Cassini. (Note that all latitudes quoted in this text are planetocentric unless otherwise specified.)

SEDs originating from lightning storms deep within Saturn's atmosphere must ultimately transit its ionosphere in order to be detected by a spacecraft. Therefore, the low frequency cutoff of each SED episode provides information about the intervening plasma densities, as only frequencies larger than the peak electron plasma frequency will pass through Saturn's ionosphere. Further complications to the SED propagation must also be considered, however. For example, the spacecraft is very rarely directly overhead the storm location; an increased angle of incidence (α) between the zenith and the direction of radio wave propagation leads to an increase in the observed cutoff frequency (e.g., Fischer et al., 2007). In addition, "over horizon" SEDs are observed regularly (Fischer et al., 2008). These types of SEDs are detected prior to their originating storm rising above the visible horizon as seen by Cassini, likely a result of ionospheric ducting (Zarka et al., 2006). This latter point emphasizes that one cannot rely on the assumption that SEDs traverse a straight line from origin to observer. Nevertheless, with careful attention to such details, SED measurements can be used to make an estimate of the peak electron density as a function of local time for Saturn's ionosphere. Such a data product is highly complementary to the only other remote sensing diagnostic of Saturn's mid- and low-latitude ionosphere, that of $N_e(h)$ profiles from radio occultation experiments (e.g., Nagy et al., 2006; Kliore et al., 2009). It is important to emphasize that Sun–Saturn–Earth geometry limits radio occultations to Saturn dawn and dusk, while SEDs can be observed at all local times.

We have focused only on summarizing the basic characteristics of SEDs as they relate to Saturn's ionosphere here. For a more complete discussion of the complications of SED generation, propagation, and detection the reader is referred to Fischer et al. (2011a) and references therein.

1.3. Voyager era studies

Kaiser et al. (1984) used Voyager SED measurements to derive a diurnal variation of the peak electron density in Saturn's ionosphere, N_{MAX}, of over two orders of magnitude. Midnight densities of less than 10^3 cm^{-3} were followed by densities in excess of 10^5 cm^{-3} at noon, with dawn and dusk densities of ~10^4 cm^{-3}, in rough agreement with the radio occultation data at those local times (e.g., Kliore et al., 1980; Lindal et al., 1985). Zarka (1985) derived a slightly larger diurnal variation using a similar analysis. Fig. 1a and b present the Voyager era SED-derived diurnal variation in N_{MAX} from Kaiser et al. (1984), and Zarka (1985), respectively.

Early theoretical models of Saturn's ionosphere predicted H^+ to be the dominant ion, with a peak density of ~10^5 cm^{-3} and a minimal diurnal variation, owing to the long lifetime of H^+ (e.g., McElroy, 1973). Based on radio occultation measurements of a 10^4 cm^{-3} ionosphere, it had already been recognized that additional losses were required in the models, such as the conversion of H^+ ions into short-lived molecular ions (Connerney and Waite, 1984). The first time-dependent model of Saturn's ionosphere to address the SED-derived diurnal variation of N_{MAX} was that of Majeed and McConnell (1996). They examined a range of possible loss chemistries and forced ion vertical drifts, and could not find any combination of parameters that would come close to reproducing the SED observations. Prior to Cassini's arrival at Saturn, Moore et al. (2004) presented a new set of model results addressing this problem. They found diurnal variations similar to those calculated by Majeed and McConnell, and further demonstrated that even the most drastic or minimal allowable chemical losses, constrained only by Voyager observations, would not lead to variations of two orders of magnitude in N_{MAX} in only 5 h (i.e., noon ↔ midnight).

Even ignoring differences in instrumentation, there are a number of advantages that Cassini has over the Voyager spacecraft when deriving peak electron densities in Saturn's ionosphere from SEDs. First, the location of the storm cloud tops has been identified for the majority of Cassini SED storm periods. This means that (a) it is easier to isolate the local solar time sampled by the SEDs as they propagate through the ionosphere, and (b) the angle of incidence is known (to an accuracy that depends inversely on the size of the originating storm). Second, whereas both Voyager spacecraft flew past Saturn in a matter of days, Cassini has been in orbit since 1 July 2004, and will continue to take data until 2017 (Spilker, 2012). Such a long term SED data set allows a more complete coverage in Saturn local time, and also allows study of new topics, such as how the SED-derived N_{MAX} diurnal variation responds to changes in solar flux and Saturn season.

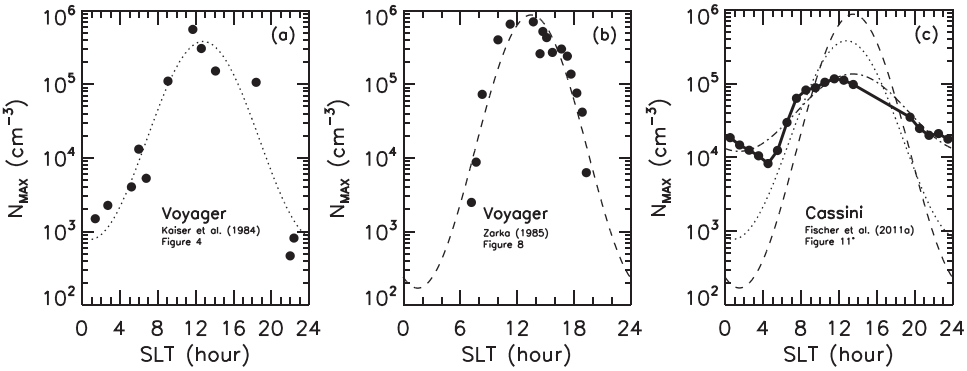

Fig. 1. Diurnal variation in N_{MAX} derived from Voyager and Cassini SED observations (circles and solid curve), along with a least-squares fit to an equation of the form $\log N_e = A - B\cos(LT - \phi)$ (the dotted, dashed and dot-dash curves). (a) Voyager: Fig. 4 of Kaiser et al. (1984), (b) Voyager: Fig. 8 of Zarka (1985), (c) Cassini: the diurnal trend from Fig. 11 of Fischer et al. (2011a). A straight line has been drawn between 13.5 LT and 19.5 LT where there is a relative lack of data (see Section 4.1). The dash-dotted line represents a fit to the Cassini data set. In addition, the dotted and dashed curves are the fits for the Kaiser et al. (1984) and Zarka (1985) diurnal N_{MAX} trends from the Voyager era, also shown in (a) and (b), respectively.

The vast majority of Cassini era SEDs detected to date originate from storm systems at 35°S latitude (Fischer et al., 2011a). However, approximately 16 months after Saturn passed through its equinox (August 2009) towards southern winter, a giant convective storm developed at 35°N latitude, accompanied by unprecedented levels of SED activity (Fischer et al., 2011b). Therefore, aside from one small storm which may have been equatorial, Cassini era SED storms have all been in the same hemisphere as the sub-solar point. While the tendency for convective storms to preferentially form near ±35° latitude remains unexplained, it is beneficial for our purposes in that it provides additional sampling of Saturn's mid-latitude ionosphere.

Using the Saturn Thermosphere Ionosphere Model (STIM), we present here the first attempt at reproducing the diurnal variation of N_{MAX} obtained from Cassini era observations. The new constraints provided by Cassini SEDs, and how they differ from the Voyager ones, are summarized in Section 2. Our model is described in Section 3. Section 4 presents the model results, and Section 5 discusses possible solutions to the model-data discrepancy. Finally, concluding thoughts are given in Section 6.

2. Diurnal variation of N_{MAX} derived from Cassini era SEDs

Comprehensive discussion of the Cassini era derivations of peak electron densities in Saturn's ionosphere to date can be found in Fischer et al. (2011a); we briefly summarize those findings here. First, while SEDs were detected by both Voyagers for the few days near closest approach, Cassini's first few years in orbit have revealed that there are distinctive storm periods separated by periods of SED quiet. Based on 48 SED episodes between 2004 and 2009, Fig. 1c shows the average diurnal variation of N_{MAX} at Saturn for measurements where Cassini was within 14 R_S of Saturn (Fischer et al., 2011a). In contrast, Voyager 1 observations are based on a few measurement points over three SED episodes, whereas Voyager 2 data showed a decline in number and intensity of SEDs with no clear episodic behavior, meaning it could not be used for a similar analysis, as the storm's position was not well defined (Kaiser et al., 1984). As seen in Fig. 9 of Fischer et al. (2011a), there is good qualitative agreement in the diurnal variations of N_{MAX} derived from the eight different Cassini storm periods. The maximum N_{MAX} value is typically in the early afternoon, while the minimum is in the mid-morning, just before sunrise, as would be expected (e.g., Moore et al., 2004). Quantitative agreement between N_{MAX} values for different SED storms is more varied: at a single local time, N_{MAX} values derived from different storms can differ by as much as a factor of ten, but are more typically within a factor of 2–3. On average, the inferred diurnal variation of N_{MAX} in the Cassini era is only a factor of ten, from $\sim 10^4$ cm^{-3} at midnight to $\sim 10^5$ cm^{-3} at noon. This is in distinct contrast to the two order of magnitude diurnal variation inferred from Voyager measurements, where N_{MAX} values fell below 10^3 cm^{-3} during the night. As no Cassini SEDs have inferred similarly low N_{MAX} values to date, the Voyager result may represent an exceptional situation. Finally, Fischer et al. (2011a) also examined trends in derived N_{MAX} values with solar EUV flux. They found a slight correlation between the diurnal variation of N_{MAX} and the EUV flux, and a stronger correlation between the average peak N_{MAX} values and the EUV flux, indicating that – as expected – solar EUV flux plays a dominant role in ionizing Saturn's mid-latitude ionosphere.

3. Modeling approach

3.1. The Saturn thermosphere ionosphere model

The Saturn Thermosphere Ionosphere Model (STIM) is a suite of 1D, 2D and 3D models of Saturn's upper atmosphere. The core of STIM is a 3D global circulation model (GCM) of the Saturn thermosphere, first described by Müller-Wodarg et al. (2006), and now updated to include a fully coupled ionosphere (Müller-Wodarg et al., 2012). Separate 1D (in altitude), and 2D (altitude and latitude) ionospheric modules exist that use the thermospheric GCM to define background atmospheric parameters not calculated by the ionospheric modules. These modules include photochemistry, plasma diffusion (Moore et al., 2004), shadowing due to Saturn's rings (Mendillo et al., 2005), and a time-variable water influx (Moore et al., 2006; Moore and Mendillo, 2007). Recently the ionospheric modules have been coupled with a 1D electron transport code in order to incorporate the effects of photoelectrons on Saturn's ionosphere (Galand et al., 2009, 2011), including plasma temperature calculations (Moore et al., 2008), and parameterizations of the secondary ionization and thermal electron heating rates at Saturn (Moore et al., 2009). Saturn's magnetic field is specified with the Saturn Pioneer Voyager (SPV) model (Davis and Smith, 1990). Calculations using updated magnetic field parameters based on Cassini measurements (e.g., Russell and Dougherty, 2010) do not show any discernible differences from those using the SPV model.

In order to reduce the calculated electron densities to better match radio occultation observations, models of Saturn's ionosphere have had to rely on a combination of charge exchange reactions that remove the long-lived ion H^+ (e.g., Majeed and McConnell, 1996; Moses and Bass, 2000). These reactions have typically been driven by some combination of an assumed influx of water (Connerney and Waite, 1984), and by some assumed fraction of atmospheric molecular hydrogen excited to the 4th or higher vibrational level, H_2^* (McElroy, 1973). As both the influx of H_2O into Saturn's atmosphere and the H_2^* population are largely unconstrained at present, previous STIM studies have explored a wide range of possibilities for those parameters (Moore et al., 2006, 2010), and compared the resulting model calculations with Cassini radio occultation observations (Nagy et al., 2006; Kliore et al., 2009) in order to find a "best" match.

The effective reaction rate k_1^* for charge exchange between H^+ and vibrationally excited H_2 is given by:

$$k_1^* = k_1 \frac{[H_2(v \geq 4)]}{[H_2]} \ [\text{cm}^3\ \text{s}^{-1}] \quad (1)$$

where the reaction rate k_1 is taken to be 1×10^{-9} cm^3 s^{-1} based on Huestis (2008), and the initial population of vibrationally excited hydrogen is taken to be that of Moses and Bass (2000). As Moses and Bass assumed a k_1 of 2×10^{-9} cm^3 s^{-1}, a factor of two larger than our rate, the base k_1^* for our calculations is 0.5 k_{1MB}^*. Any further modifications to k_1^* throughout this text refer to modifications of this population of vibrationally excited molecular hydrogen, $[H_2(v \geqslant 4)]$, and not the reaction rate k_1 or the background density $[H_2]$.

Based on model comparisons (Moore et al., 2010) with the latitudinal variation of N_{MAX} from radio occultations (Kliore et al., 2009), the water influxes used in this study assume a Gaussian distribution with latitude, peaked at Saturn's equator, with a variance of 10° latitude. This means that at 35°S latitude, where SED comparison calculations take place, a peak water influx of 5×10^6 H_2O molecules cm^{-2} s^{-1} (i.e., at the equator) would be reduced to $\sim 1.1 \times 10^4$ cm^{-2} s^{-1} – a value too low to significantly affect ionospheric electron densities. Only the peak water influx at the equator Φ_{eq} is discussed for the remainder of the text, with the above distribution in latitude assumed.

Saturn's lower ionosphere is predicted to be composed of a complex array of hydrocarbon ions which provide an additional ledge of ionization between Saturn's main photochemical peak and the homopause (Moses and Bass, 2000). STIM does not include the hundreds of reactions necessary to fully apportion accurate hydrocarbon ion fractions; rather it uses a small subset of

simplified chemistry that acts predominantly as a sink for Saturn's major ions, H^+ and H_3^+. Though the ultimate hydrocarbon ions in STIM's chemical scheme – CH_3^+, CH_4^+, and CH_5^+, hereafter designated CH_X^+ – are different from those that result from a more complete treatment (e.g., $C_3H_5^+$ of Moses and Bass, 2000), the calculated electron density in the hydrocarbon region is approximately unchanged (Moore et al., 2008).

3.2. Simulations of diurnal variation in electron density

The background neutral atmosphere, upon which the 1D ionospheric calculations are based, comes from the 3D GCM, which calculates the self-consistent temperatures, winds, and composition resulting from external energy inputs (Müller-Wodarg et al., 2006). While there now exists an updated version of the GCM (Müller-Wodarg et al., 2012), we have chosen to maintain consistency with previous publications by using the GCM background described by Moore et al. (2010). In brief, this simulation is for solar minimum conditions at Saturn equinox, and reproduces neutral temperature measurements in the UV (Smith et al., 1983; Nagy et al., 2009) and IR (Melin et al., 2007). Altitude profiles of neutral densities and temperatures from this background atmosphere are presented in Fig. 2. Vertical transport of ions due to neutral winds is also included in the ionospheric calculations, though as the resulting timescales are larger than those due to chemical loss their impact is negligible over the altitude range considered here (Moore et al., 2004), and therefore they are not shown.

The solar declination angle for the 1D ionospheric module calculations is fixed at −8.5°, representing the average seasonal condition for the 31 radio occultation observations published to date (Nagy et al., 2006; Kliore et al., 2009), and also a fair approximation to the average condition for Cassini era SED storms (Fischer et al., 2011a). Solar flux at the top of the atmosphere is based on similar average conditions, specified using the measurements from the Thermosphere Ionosphere Mesosphere Energetics and Dynamics Solar EUV Experiment (TIMED/SEE) extrapolated to Saturn (Woods et al., 2000, 2005; Woods, 2008).

4. Results: modeled diurnal variations of electron density

4.1. Nominal predictions and expected trends

Fig. 3 presents the nominal model result, based on previous comparisons with radio occultation observations, for the same conditions described in Fig. 4 of Moore et al. (2010): 0.125 k_1^* and Φ_{eq} of 5×10^6 cm^{-2} s^{-1}. Note that this is actually identical to the $0.25k_1^*$ quoted by Moore et al. (2010), as they describe the reduction to the k_1 reaction rate (by a factor of two) separately from the modification to the population of vibrationally excited H_2, whereas here we incorporate it directly into Eq. (1). Peak electron density is shown versus solar local time along with the peak densities of the major ion species. The four radio occultations nearest in latitude to 35°S are also shown, two at dawn (047x and 051x, open circles) and two at dusk (051n and 054n, asterisks). Table 1 of Kliore et al. (2009) describes the full details of these occultations. Modeled N_{MAX} values are within a factor of two of those from radio occultations. A better model-data agreement could be found for these four observations; however, the model parameters responsible for Fig. 3 are based on a comparison with all 31 Cassini radio occultation profiles (Moore et al., 2010). Finally, two diurnal profiles of N_{MAX} derived from Cassini SEDs are also shown in Fig. 3: they are from Fig. 9 (dotted curve) and Fig. 11 (dashed curve) of Fischer et al. (2011a), respectively. The dotted curve represents the Cassini N_{MAX} value when all 231 SED episodes are averaged together, whereas the dashed curve limits the determination of N_{MAX} to only SEDs observed when Cassini was within 14 R_S of Saturn. Fischer et al. (2011a) found a slight dependence of the cutoff frequency on spacecraft distance (see their Fig. 3), and those profiles with Cassini nearest to Saturn can be considered as more accurate as the SED intensities are higher. The near-distance profiles (i.e. their Fig. 11) exhibit a clear minimum in the early morning, just before sunrise. Afternoon local times suffer from a lack of data, however, and a straight line has been assumed for the N_{MAX} profile between the 13.5 SLT and 19.5 SLT intervals (represented in Fig. 3 by a thin dashed line).

In order to give some sense of the relevant vertical structure in Saturn's ionosphere, the same model simulation and observations from Fig. 3 are shown as altitude profiles in Fig. 4. Though the two dawn radio occultations plotted here (047x and 051x) have high-altitude electron density peaks, they represent exceptions to the average mid-latitude ionosphere measured by Cassini, which

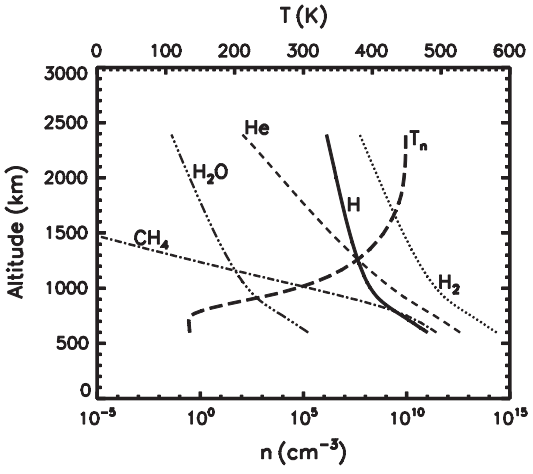

Fig. 2. Background neutral atmospheric densities and temperature, extracted from the 3D GCM for 35°S latitude at local noon. Also shown is the water density profile calculated at 35°S latitude for $\Phi_{eq} = 5 \times 10^6$ cm^{-2} s^{-1}.

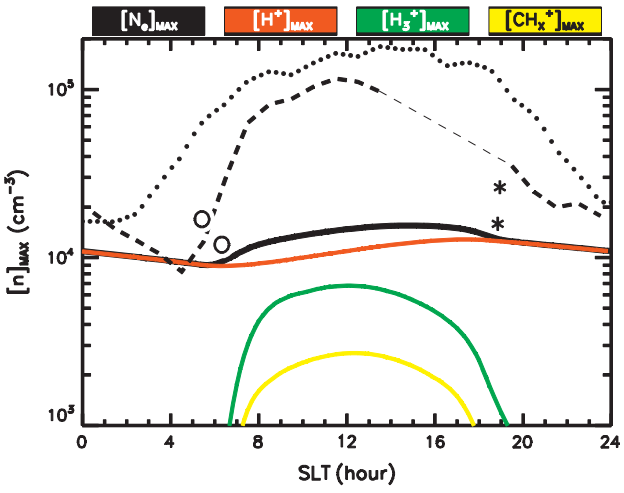

Fig. 3. Nominal STIM results for 35°S latitude, with a solar flux and declination representative of Cassini era averages, using 0.125 k_1^* and $\Phi_{eq} = 5 \times 10^6$ cm^{-2} s^{-1}. Diurnal variation of peak electron density (N_{MAX}) is given by the black solid curve; red, green and yellow curves represent the peak densities of the H^+, H_3^+ and $CH_X^+ (= CH_3^+ + CH_4^+ + CH_5^+)$ ion species, respectively. Also shown are the peak electron densities from the four Cassini radio occultation observations nearest to 35°S latitude (047x, 051x, 051n, and 054n; Kliore et al., 2009), with open circles for dawn and asterisks for dusk. Finally, the diurnal variation of N_{MAX} derived from Cassini SEDs is also plotted here as dotted and dashed curves (Figs. 9 and 11, respectively; Fischer et al., 2011a). (For interpretation of the references to colour in this figure legend, the reader is referred to the web version of this article.)

has an h_{MAX} near 1200 km (Kliore et al., 2009). Their electron density minima near 2000 km are also unusual features. Sharp low-altitude plasma layers, below ~1000 km altitude, appear in the radio occultation data. None of the mechanisms proposed to generate these low-altitude layers (discussed in Section 5.1) have been incorporated into STIM yet, which explains the model-data discrepancies there. Finally, SED-derived N_{MAX} values are extracted for the four plotted local times, and their values indicated in Fig. 4. These values come from Fig. 11 of Fischer et al. (2011a), and therefore the plotted dusk value is based on the straight line interpolation discussed above.

As the peak value of individual ion species does not necessarily occur at the altitude of the peak electron density, h_{MAX}, Fig. 5 shows the variation in the peak altitude of each ion species, as well as the diurnal variation of h_{MAX}. For these simulation conditions, H^+ is the dominant ion near the electron density peak; this shows up clearly in Fig. 3, and is the reason the red (H^+) and black (e^-) curves track each other so closely in Fig. 5. Dissociative recombination with electrons is the dominant loss of H_3^+. Therefore, as h_{MAX} remains below 1500 km, the increase in the altitude of the H_3^+ peak during the Saturn night is explained by a relatively larger low altitude loss rate leading to a high altitude ion ledge just after sunset. Fig. 5 serves as a reminder that while we plot peak ion densities in Figs. 3 and 6, they are at a range of altitudes that can differ from h_{MAX}.

4.2. Saturn ionospheric photochemistry

Photoionization of molecular hydrogen is the dominant source of ion production in Saturn's mid-latitude ionosphere.

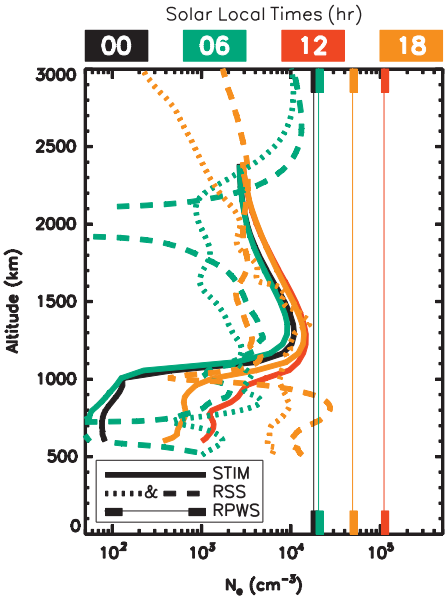

Fig. 4. Altitude profiles of electron density for the same simulation conditions and Cassini observations shown in Fig. 3. All plotted values are color coded according to their representative local time: black for midnight (00 SLT), green for dawn (06 SLT), red for noon (12 SLT), and orange for dusk (18 SLT). Thick solid lines represent nominal STIM results. Thick dashed lines show the four Cassini radio occultation observations nearest to 35°S latitude (047x, 051x, 051n, and 054n; Kliore et al., 2009), where the short-dash and long-dash are used only to distinguish between the two profiles at dawn or dusk, respectively. Finally, SED-derived N_{MAX} values are indicated by thick bars at the top and bottom of the plot, with a thin line drawn between them to make comparisons with the radio occultation values easier (taken from Fig. 11 of Fischer et al. (2011a)). Note that the dusk SED-derived value for N_{MAX} represents an interpolation as discussed in the text. (For interpretation of the references to color in this figure legend, the reader is referred to the web version of this article.)

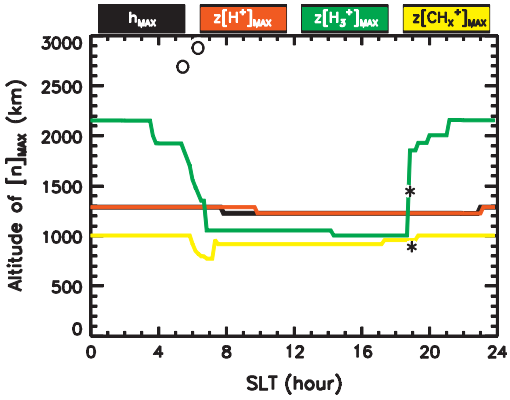

Fig. 5. Nominal STIM results for 35°S latitude, with a solar flux and declination representative of Cassini era averages, using 0.125 k_1^* and $\Phi_o = 5 \times 10^6$ cm^{-2} s^{-1}. Diurnal variation of the altitude of the peak electron density (h_{MAX}) is shown in black; red, green and yellow curves represent the altitudes of the peak densities of the H^+, H_3^+ and CH_x^+ ($= CH_3^+ + CH_4^+ + CH_5^+$) ion species, respectively. Also shown are the h_{MAX} values from the four Cassini radio occultation observations nearest to 35°S latitude (047x, 051x, 051n, and 054n; Kliore et al., 2009). (For interpretation of the references to colour in this figure legend, the reader is referred to the web version of this article.)

Approximately 90% of the primary ions produced through absorption of photons are H_2^+, with the remaining 10% of photo ion production accounting for, in descending order, H^+, He^+ and hydrocarbon ions. The relatively fast charge exchange reaction, $H_2^+ + H_2 \rightarrow H_3^+ + H$, means that, effectively, H_3^+ is the ion most readily produced in Saturn's ionosphere. Slower production, but typically also slower loss, allows H^+ to build up over the course of a few Saturn days, eventually competing with H_3^+ for dominance in a steady state diurnal solution. The mix of long-lived atomic and short-lived molecular ions drives the diurnal variation in electron density. As shown by Moore et al. (2004), the H^+/H_3^+ ratio is proportional to electron density in photochemical equilibrium, which they also demonstrate to hold up to ~2300 km in Saturn's mid-latitude ionosphere. Therefore, for conditions dominated by H^+, previous ionospheric models all predicted a minimal diurnal variation in N_{MAX}. On the other hand, in an H_3^+ dominated ionosphere, the relatively low photoionization rate at Saturn (i.e., at ~10 AU) led to an N_{MAX} smaller than derived from SEDs (e.g., Majeed and McConnell, 1996; Moses and Bass, 2000; Moore et al., 2004).

In order to illustrate the difficulty presented in reproducing the SED-derived diurnal trend in N_{MAX}, we consider the following basic calculations. First, the peak photoionization rate at Saturn during solar maximum conditions for overhead illumination (i.e., at the sub-solar point) is ~10 cm^{-3} s^{-1} (Moore et al., 2004). If we take this maximum production rate to be fixed, and we assume that there are no ion losses whatsoever, then it would still take 2.5 h (5.6 Saturn hours) to go from an electron density of 10^4–10^5 cm^{-3}. Therefore, for Saturn photochemistry to be able to explain the SED observations, there needs to be a much larger production rate than what is currently estimated. If we instead start with an electron density of 10^5 cm^{-3}, and require it to decay to 10^4 cm^{-3} in ~6 Saturn hours (e.g., Fig. 9 of Fischer et al., 2011a), then a different problem presents itself. At 300 K, the approximate temperature near the ionization peak (e.g., Nagy et al., 2009), the H_3^+ dissociative recombination rate is on the order of 10^{-7} cm^3 s^{-1}, which means that the decay from 10^5 cm^{-3} to 10^4 cm^{-3} would take only ~30 Saturn minutes, while the full 6 Saturn hours would find an ionosphere of 10^3 cm^{-3}, too low based on Cassini SED observations. In summary, the largest estimated ion production rate is clearly not large enough to match the dawn-to-noon increase in N_{MAX} derived from SEDs, while a slower ion loss rate is required to match the dusk-to-midnight decay. Certainly, H^+ would be

expected to have a much slower decay than H_3^+; however its production rate is roughly a factor of 10 smaller than that of H_3^+, which would further exacerbate the dawn-to-noon discrepancy.

4.3. Best match to SED-derived diurnal variation of N_{MAX}

Fig. 3 represents a nearly minimal loss simulation. In other words, the two loss processes that are not well constrained – charge exchange of H^+ with H_2O and $H_2(v \geqslant 4)$ – are already at low values compared with many previous estimates. Even so, the modeled N_{MAX} values are significantly lower than those derived from Cassini era SED observations. Simulations using an increased solar flux will naturally lead to larger N_{MAX} values, though still not as large as those derived from SEDs (about a factor of two difference in N_{MAX} is expected between solar minimum and solar maximum conditions; Moore et al., 2004). More importantly, those larger fluxes are not justified here, as the measurements were made during a prolonged solar minimum period for which the average F10.7 was ~80 (as measured at Earth). As argued in Section 4.2, the diurnal variation of N_{MAX} derived from SEDs requires both extremely large production rates and loss rates within one Saturn day. Therefore, in the following we show the result of allowing for a wide range of production and loss rates (ranging from likely to unrealistic) in order to attempt and answer the question: What does it take to reproduce the SED observations?

Table 1 summarizes the parameter space explored by the 405 individual 1D model simulations that were performed in order to find the combination best able to match the SED results. The absolute range of each parameter in Table 1 is described by the minimum and maximum values, while the number of different values explored for those parameters is given below. Note that the step sizes are variable, with a higher concentration of simulations exploring parameters near those that come closest to the SED-derived diurnal variation of N_{MAX}. This results in fewer total model runs than might be expected from the number of values evaluated for each parameter.

Fig. 6 shows the model simulation that was best able to reproduce the diurnal variation of N_{MAX}, as derived from Cassini SEDs. Though it is a non-unique solution, it is illustrative of the changes in Saturn photochemistry that would be required in order to match the observations. The ion production rate – originally due to photoionization and secondary production – has been increased by a factor of 60. In order to balance this unphysical production rate, loss rates have also increased significantly: the simulation uses 20 k_1^* and $\Phi_{eq} = 2.7 \times 10^9\ cm^{-2}\ s^{-1}$ (i.e., the water influx at 35°S is $6 \times 10^6\ cm^{-2}\ s^{-1}$). Without an increase in the nominal ion production rates, it would not be possible to go from $10^4\ e^-\ cm^{-3}$ at sunrise to $\sim 10^5\ e^-\ cm^{-3}$ at noon – a short ~6 Saturn hours, or ~2.6 h. On the other hand, without an increase in the ion loss rates to balance the enhanced production rates, Saturn's ionosphere would have effectively zero diurnal variation. As the parameters used in Fig. 6 are clearly well outside of the current best estimates, we regard them as indications that SEDs are not sampling Saturn's photochemical peak ionosphere, and do not attempt to justify them further. Instead, in Section 5 we evaluate alternative explanations to SED observations.

5. Discussion: other explanations of the SED-inferred diurnal variation of N_{MAX}

The comparisons performed above rely on a number of implicit assumptions, such as: (1) the N_{MAX} value derived from SEDs is representative of the "main" ionospheric peak at Saturn, and (2) the low frequency cutoff observed in SEDs occurs in the portion of the ionosphere directly between the convective storm system and the Cassini spacecraft. As it is clear now that the diurnal variation of N_{MAX} derived from Cassini SED observations can only be reproduced chemically using non-physical ion productions and losses, it is worthwhile to examine those assumptions more closely.

Table 1
Range of simulation parameters.

	k_1^* factor[a]	Φ_{eq} ($cm^{-2}\ s^{-1}$)[b]	P[c]
Minimum	1	1×10^6	1
Maximum	30	4×10^{12}	225
N steps	10	21	13

[a] See Eq. (1).
[b] The water influx at Saturn's equator; as discussed in 3.1, the influx at 35°S latitude is ~0.22% of Φ_{eq}.
[c] An assumed increase to the ion production rates calculated in the model.

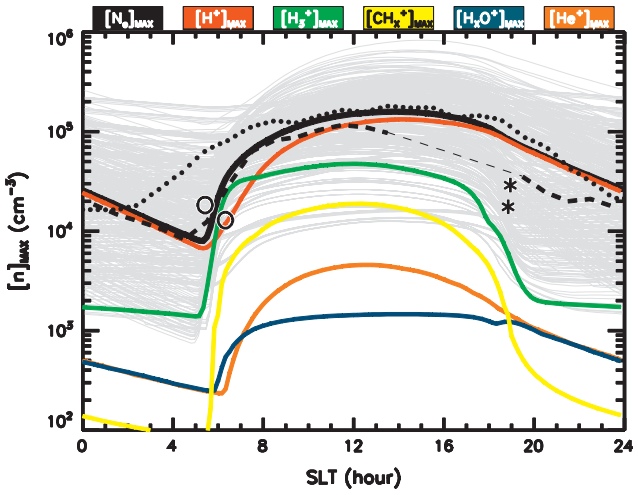

Fig. 6. Model simulation (thick solid lines) that comes closest to reproducing the diurnal variation of N_{MAX} derived from Cassini SEDs (dotted line, Fig. 9 of Fischer et al. (2011a); dashed line, Fig. 11 of Fischer et al. (2011a)). Calculations are for 35°S latitude, with a solar flux and declination representative of Cassini era averages. Both the production and loss rates have been significantly enhanced: $P = 60\ P_o$, 20 k_1^* and $\Phi_{eq} = 2.7 \times 10^9\ cm^{-2}\ s^{-1}$. Diurnal variation of the peak electron density (N_{MAX}) is shown in black; red, green, yellow, blue, and orange curves represent the peak densities of the $H^+, H_3^+, CH_X^+ (= CH_3^+ + CH_4^+ + CH_5^+), H_XO + (= H_2O^+ + H_3O^+)$, and He^+ ion species, respectively. Gray curves represent the diurnal variation of N_{MAX} from each of the 405 model simulations. Also shown are the N_{MAX} values from the four Cassini radio occultation observations nearest to 35°S latitude (Kliore et al., 2009). (For interpretation of the references to color in this figure legend, the reader is referred to the web version of this article.)

5.1. Low-altitude plasma layers

The assumption that the N_{MAX} value derived from SEDs is representative of the "main" ionospheric peak is particularly important, as the degree of variability seen in the radio occultations of Saturn's ionosphere is so large that it is difficult to even define a "main" ionospheric peak, except on average (Nagy et al., 2006; Kliore et al., 2009). Moreover, just as at Jupiter (e.g., Yelle and Miller, 2004), a majority of radio occultations of Saturn's ionosphere reveal many sharp layers of electron density, especially in the lower ionosphere, and it is quite common for the peak electron density to be within one of these layers. A radio wave traversing Saturn's ionosphere is only sensitive to the maximum plasma density, not the location of that density, so it is certainly possible that SEDs are sampling low-altitude sharp ionospheric layers, at least some of the time.

Though the origin and evolution of Saturn's sharp ionospheric layers remain largely unstudied, a number of possible explanations have been proposed. For example, Moses and Bass (2000) are able to reproduce the Voyager 2 layers near 1000 km by introducing a shear of -2 cm s^{-1} km^{-1} in the vertical plasma drift to act on magnesium (from dust grains) being deposited in the 790–1290 km region. Such shear could be the result of ion transport driven by a vertically varying neutral horizontal wind, such as would result from atmospheric gravity waves. Matcheva et al. (2001) demonstrated that gravity waves were capable of creating sharp peaks of electron density similar to those observed by Galileo at Jupiter, and Barrow and Matcheva (2011) greatly expanded this result, though no similar study has yet been published at Saturn. Even without significant shear, metallic ions from meteor ablation can lead to sharp electron density layers at low altitudes, especially near dawn (Kim et al., 2001). Finally, plasma instabilities may also play a role in forming ionospheric layers, though initial estimates of Rayleigh–Tayler growth periods are $\sim$4 h, comparable to the entire night, meaning they would not be expected to drive large-scale ionospheric structures at Saturn (Mendillo et al., 2008).

Regardless of their origin, there are a number of conditions that must be met for these low-altitude layers to be able to explain the N_{MAX} values derived from SEDs. First, either their densities must vary significantly with local time or they must be present only during the Saturn day. This latter condition represents the possibility that SEDs are sampling unusually large electron densities from sharp ionospheric layers during the day and sampling Saturn's "main" ionosphere at night. Second, their densities must correlate with solar flux, as both the SED-derived diurnal variation and peak N_{MAX} value were shown to correlate with solar EUV flux by Fischer et al. (2011a). Third, they must be able to be generated at a wide range of latitudes, as sharp low-altitude layers are present in Cassini radio occultations spanning $-74.1°$ to $75.4°$ planetographic latitude (Kliore et al., 2009). Finally, they must be generated on either a constant or a diurnal basis, as all SED storm periods find daytime peak electron densities in excess of 10^5 cm^{-3} (Kaiser et al., 1984; Zarka, 1985; Fischer et al., 2011a).

5.2. Ring shadowing

Burns et al. (1983) first posited that the shadows cast by Saturn's rings on its atmosphere may reduce the local insolation, leading to depleted electron densities, and thereby providing a possible explanation of the extremely low frequency cutoffs observed by Voyager. This effect was later studied in more detail, using STIM to calculate the shadowing effects for both the Voyager and the Cassini eras (Mendillo et al., 2005). The ring shadowing "solution" to the SED observations essentially relied on the assumption that SEDs could originate from a range of positions on the planet, and then be ducted throughout the ionosphere before reaching the detecting spacecraft. Low frequency cutoffs represented radio waves escaping through ionospheric "holes" caused by ring shadowing, while high frequency cutoffs represented occasions where the observed radio waves did not make it to any holes before transiting Saturn's ionosphere.

With the Cassini era, however, the situation changed significantly. First, Cassini was able to identify the location of the SED storms (Dyudina et al., 2007, 2010). This meant that it was possible to disentangle the path of propagation of the SEDs to some degree of accuracy. For example, when Cassini was directly above a storm there would be no ambiguity regarding the portion of Saturn's ionosphere sampled by the SEDs detected. Second, peak electron densities derived from Cassini low frequency cutoffs were nearly always above 10^4 cm^{-3}, and never as low as 10^3 cm^{-3} (Fischer et al., 2011a). Fischer et al. note that Saturn kilometric radiation (SKR) usually dominates the 300–600 kHz frequency band, possibly contaminating the detection of the 10^3 cm^{-3} low frequency cutoffs there. Regardless, the fact that Cassini has not detected such low nighttime electron densities negates the need for any ring shadowing effects to explain them. It also implies that either ring shadowing cannot reduce Cassini era electron densities to 10^3 cm^{-3}, contrary to earlier predictions (e.g., Mendillo et al., 2005), or that SEDs are not able to travel such far distances before escaping through Saturn's ionosphere. Finally, it should be noted that the Cassini era SED storms (35°S prior to equinox in August 2009, 35°N thereafter) have always been located in the opposite hemisphere from the ring shadowing. There was one exception – an SED storm in the first half of 2010 at 35°S – but it was also located far away from the ring shadow with derived N_{MAX} values in agreement with earlier Cassini storms.

In summary, while shadows cast by Saturn's rings could have affected the ionospheric densities sampled by the equatorial storm of Voyager era SEDs, it seems unlikely that ring shadowing has played any role for Cassini era SED observations. Therefore, any explanation of the SED-derived N_{MAX} values should be applicable whether or not ring shadowing effects are present.

5.3. Plasma dynamics

Dynamical processes may also impact the electron densities sampled by SEDs, however the location of the associated storms limits these possibilities significantly. For instance, the majority of the Cassini era SEDs originate from 35°S latitude, which is magnetically connected to Saturn's C ring at about 1.44 R_S, so it is tempting to imagine a plasma interchange process occurring between Saturn's ionosphere and ring plane (e.g., Connerney, 1986). A completely different process would still be required to explain Voyager era SEDs, however, as they most likely originated from an equatorial storm system with no magnetic connection to Saturn's rings. If a dynamical plasma process is invoked to reproduce diurnal variations of N_{MAX} from SEDs, it must work equally well at both mid- and low-latitudes, for both solar minimum and solar maximum flux conditions, and for conditions with and without ring shadowing.

6. Summary

We have presented the most comprehensive modeling study to date (405 simulation runs) of the diurnal variation of N_{MAX} derived from Cassini era SEDs. The main conclusions are summarized as follows:

(1) No combination of Saturn photochemistry can explain the SED observations when parameters are limited to their observed constraints.
(2) Only by introducing artificially large production and loss processes can a model of Saturn's photochemical peak reproduce SED observations.
(3) SEDs may instead be sampling the highly variable, sharp plasma layers frequently observed in Saturn's lower ionosphere, provided those layers fulfill certain observational constraints.
(4) Ring shadowing, first introduced to help explain extremely low N_{MAX} values from Voyager SEDs, is unlikely to play a role in the Cassini era.

Taken together, the first two conclusions are a strong indication that SEDs may not be sampling Saturn's "main" ionosphere. It is unlikely that calculated photoionization rates are off by the factor of 60 used in Fig. 6, as they are based on solar fluxes that have been demonstrated to work well at Earth, and models are able to

reproduce the electron densities from radio occultations of Saturn's atmosphere with much greater accuracy. Similarly, though H_2^* and H_2O densities are not completely constrained at Saturn, the extreme values used in generating Fig. 6 are significantly larger than any previous estimates or observations.

The frequency with which low altitude electron density layers are observed in radio occultations of Saturn (and Jupiter), and the fact that they often represent N_{MAX}, lends additional credibility to the possibility that SEDs are sampling these highly variable layers. For such an explanation of the diurnal variation of N_{MAX} derived from SEDs to hold weight, however, it must be demonstrated that they do not violate any of the current observational constraints. For example, atmospheric gravity waves may indeed be acting to create such ionospheric structures, as at Jupiter (Barrow and Matcheva, 2011), but: (a) Are they present at all times during the day and depleted at night? (b) Do their peak densities correlate with solar EUV flux? (c) Are they present at a wide range of latitudes and are they present on a near constant basis? Moreover, if gravity waves are responsible for Saturn's sharp low-altitude layers of electron density: do the wave amplitudes and periods required to generate N_{MAX} values that correspond to those derived from SEDs violate any other observational constraints? In short, while it is tempting to use these plasma layers as an explanation of the SED observations, it is yet far from clear that they can do so adequately.

Acknowledgments

We are grateful to the TIMED/SEE PI Tom Woods, and his team for providing us with the solar flux data set and associated routines for extrapolation to planets. We acknowledge the contribution of the International Space Sciences Institute (ISSI) in Bern, Switzerland, for hosting and funding the ISSI International Team on Saturn Aeronomy (166) and the constructive discussions by colleagues attending the meetings. Funding for this work at Boston University comes from the NASA CDAP Program. G.F. was supported by a grant (Project P21295-N16) from the Austrian Science Fund (FWF) and by a short-term research scholarship at the University of Iowa funded by NASA through contract 1356500 from the Jet Propulsion Laboratory. Partial support for M.G. and I.M.W. comes from the Science and Technology Facilities Council (STFC) rolling grant to Imperial College London.

References

Barrow, D., Matcheva, K.I., 2011. Impact of atmospheric gravity waves on the jovian ionosphere. Icarus 211, 609–622.
Burns, J.A., Showalter, M.R., Cuzzi, J.N., Durisen, R.H., 1983. Saturn's electrostatic discharges – Could lightning be the cause? Icarus 54, 280–295.
Connerney, J.E.P., 1986. Magnetic connection for Saturn's rings and atmosphere. Geophys. Res. Lett. 13, 773–776.
Connerney, J.E.P., Waite, J.H., 1984. New model of Saturn's ionosphere with an influx of water from the rings. Nature 312, 136–138.
Davis Jr., L., Smith, E.J., 1990. A model of Saturn's magnetic field based on all available data. J. Geophys. Res. 95, 15257–15261.
Dyudina, U.A. et al., 2007. Lightning storms on Saturn observed by Cassini ISS and RPWS during 2004–2006. Icarus 190, 545–555.
Dyudina, U.A. et al., 2010. Detection of visible lightning on Saturn. Geophys. Res. Lett. 37, L09205. http://dx.doi.org/10.1029/2010GL043188.
Evans, D.R., Warwick, J.W., Pearce, J.B., Carr, T.D., Schauble, J.J., 1981. Impulsive radio discharges near Saturn. Nature 292, 716–718.
Evans, D.R., Romig, J.H., Hord, C.W., Simmons, K.E., Warwick, J.W., Lane, A.L., 1982. The source of Saturn electrostatic discharges. Nature 299, 236–237.
Fischer, G. et al., 2006. Saturn lightning recorded by Cassini/RPWS in 2004. Icarus 183, 135–152.
Fischer, G. et al., 2007. Analysis of a giant lightning storm on Saturn. Icarus 190, 528–544.
Fischer, G. et al., 2008. Atmospheric electricity at Saturn. Space Sci. Rev. 137, 271–285.
Fischer, G., Gurnett, D.A., Zarka, P., Moore, L., Dyudina, U.A., 2011a. Peak electron densities in Saturn's ionosphere derived from the low-frequency cutoff of Saturn lightning. J. Geophys. Res. (Space Phys.) 116, A04315. http://dx.doi.org/10.1029/2010JA016187.
Fischer, G. et al., 2011b. A giant thunderstorm on Saturn. Nature 475, 75–77.
Galand, M., Moore, L., Charnay, B., Müller-Wodarg, I., Mendillo, M., 2009. Solar primary and secondary ionization at Saturn. J. Geophys. Res. (Space Phys.) 114, A06313. http://dx.doi.org/10.1029/2008JA013981.
Galand, M., Moore, L., Müller-Wodarg, I., Mendillo, M., Miller, S., 2011. Response of Saturn's auroral ionosphere to electron precipitation: Electron density, electron temperature, and electrical conductivity. J. Geophys. Res. (Space Phys.) 116, A09306. http://dx.doi.org/10.1029/2010JA016412.
Huestis, D.L., 2008. Hydrogen collisions in planetary atmospheres, ionospheres, and magnetospheres. Planet. Space Sci. 56, 1733–1743.
Kaiser, M.L., Connerney, J.E.P., Desch, M.D., 1983. Atmospheric storm explanation of saturnian electrostatic discharges. Nature 303, 50–53.
Kaiser, M.L., Desch, M.D., Connerney, J.E.P., 1984. Saturn's ionosphere: Inferred electron densities. J. Geophys. Res. 89 (A4), 2371–2376.
Kim, Y.H., Pesnell, W.D., Grebowsky, J.M., Fox, J.L., 2001. Meteoric ions in the ionosphere of Jupiter. Icarus 150, 261–278.
Kliore, A.J. et al., 1980. Structure of the ionosphere and atmosphere of Saturn from Pioneer 11 Saturn radio occultation. J. Geophys. Res. 85 (A11), 5857–5870.
Kliore, A.J. et al., 2009. Midlatitude and high-latitude electron density profiles in the ionosphere of Saturn obtained by Cassini radio occultation observations. J. Geophys. Res. (Space Phys.) 114, A04315. http://dx.doi.org/10.1029/2008JA013900.
Lindal, G.F., Sweetnam, D.N., Eshleman, V.R., 1985. The atmosphere of Saturn: An analysis of the Voyager radio occultation measurements. Astron. J. 90, 1136–1146.
Majeed, T., McConnell, J.C., 1996. Voyager electron density measurements on Saturn: Analysis with a time dependent ionospheric model. J. Geophys. Res. 101, 7589–7598.
Matcheva, K.I., Strobel, D.F., Flasar, F.M., 2001. Interaction of Gravity Waves with ionospheric plasma: Implications for Jupiter's ionosphere. Icarus 152, 347–365.
McElroy, M.B., 1973. The ionospheres of the major planets. Space Sci. Rev. 14, 460–473.
Melin, H., Miller, S., Stallard, T., Trafton, L.M., Geballe, T.R., 2007. Variability in the H_3^+ emission of Saturn: Consequences for ionisation rates and temperature. Icarus 186, 234–241.
Mendillo, M., Moore, L., Clarke, J., Müller-Wodarg, I., Kurth, W.S., Kaiser, M.L., 2005. Effects of ring shadowing on the detection of electrostatic discharges at Saturn. Geophys. Res. Lett. 32, L05107. http://dx.doi.org/10.1029/2004GL021934.
Mendillo, M. et al., 2008. Can equatorial spread-F (ESF) occur on other planets? ISEA 2008. Abstract S6-P2-31.
Moore, L., Mendillo, M., 2007. Are plasma depletions in Saturn's ionosphere a signature of time-dependent water input? Geophys. Res. Lett. 34, L12202. http://dx.doi.org/10.1029/2007GL029381.
Moore, L.E., Mendillo, M., Müller-Wodarg, I.C.F., Murr, D.L., 2004. Modeling of global variations and ring shadowing in Saturn's ionosphere. Icarus 172, 503–520.
Moore, L., Nagy, A.F., Kliore, A.J., Müller-Wodarg, I., Richardson, J.D., Mendillo, M., 2006. Cassini radio occultations of Saturn's ionosphere: Model comparisons using a constant water flux. Geophys. Res. Lett. 33, L22202. http://dx.doi.org/10.1029/2006GL027375.
Moore, L., Galand, M., Müller-Wodarg, I., Yelle, R., Mendillo, M., 2008. Plasma temperatures in Saturn's ionosphere. J. Geophys. Res. (Space Phys.) 113, A10306. http://dx.doi.org/10.1029/2008JA013373.
Moore, L., Galand, M., Müller-Wodarg, I., Mendillo, M., 2009. Response of Saturn's ionosphere to solar radiation: Testing parameterizations for thermal electron heating and secondary ionization processes. Planet. Space Sci. 57, 1699–1705.
Moore, L., Müller-Wodarg, I., Galand, M., Kliore, A., Mendillo, M., 2010. Latitudinal variations in Saturn's ionosphere: Cassini measurements and model comparisons. J. Geophys. Res. (Space Phys.) 115, A11317. http://dx.doi.org/10.1029/2010JA015692.
Moses, J.I., Bass, S.F., 2000. The effects of external material on the chemistry and structure of Saturn's ionosphere. J. Geophys. Res. 105, 7013–7052.
Müller-Wodarg, I.C.F., Mendillo, M., Yelle, R.V., Aylward, A.D., 2006. A global circulation model of Saturn's thermosphere. Icarus 180, 147–160.
Müller-Wodarg, I.C.F., Moore, L., Galand, M., Mendillo, M., 2012. Magnetosphere–atmosphere coupling at Saturn: 1. Response of thermosphere and ionosphere to steady state polar forcing. Icarus, submitted for publication. http://dx.doi.org/10.1016/j.icarus.2012.08.034.
Nagy, A.F. et al., 2006. First results from the ionospheric radio occultations of Saturn by the Cassini spacecraft. J. Geophys. Res. (Space Phys.) 111, A06310. http://dx.doi.org/10.1029/2005JA011519.
Nagy, A.F. et al., 2009. Upper atmosphere and ionosphere of Saturn. In: Dougherty, M.K., Esposito, L.W., Krimigis, S.M. (Eds.), Saturn from Cassini–Huygens. Springer, New York, pp. 181–202.
Porco, C.C. et al., 2005. Cassini imaging science. Initial results on Saturn's atmosphere. Science 307, 1243–1247.
Russell, C.T., Dougherty, M.K., 2010. Magnetic fields of the outer planets. Space Sci. Rev. 152, 251–269.
Smith, G.R., Shemansky, D.E., Holberg, J.B., Broadfoot, A.L., Sandel, B.R., McConnell, J.C., 1983. Saturn's upper atmosphere from the Voyager 2 EUV solar and stellar occultations. J. Geophys. Res. 88, 8667–8678.
Spilker, L.J., 2012. Cassini: Science highlights from the equinox and solstice missions. Lunar Planet. Sci. 43, 1358 (abstract).
Tyler, G.L. et al., 1981. Radio science investigations of the Saturn system with Voyager 1 – Preliminary results. Science 212, 201–206.

Warwick, J.W. et al., 1981. Planetary radio astronomy observations from Voyager 1 near Saturn. Science 212, 239–243.
Warwick, J.W. et al., 1982. Planetary radio astronomy observations from Voyager 2 near Saturn. Science 215, 582–587.
Woods, T.N., 2008. Recent advances in observations and modeling of the solar ultraviolet and X-ray spectral irradiance. Adv. Space Res. 42, 895–902.
Woods, T. et al., 2000. TIMED solar EUV experiment. Phys. Chem. Earth C 25, 393–396.
Woods, T.N. et al., 2005. Solar EUV experiment (SEE): Mission overview and first results. J. Geophys. Res. (Space Phys.) 110, A01312. http://dx.doi.org/10.1029/2004JA010765.
Yelle, R.V., Miller, S., 2004. Jupiter's thermosphere and ionosphere. In: Bagenal, F., Dowling, T.E., McKinnon, W.B. (Eds.), Jupiter: The Planet, Satellites and Magnetosphere. Cambridge Univ. Press, New York, pp. 185–218.
Zarka, P., 1985. Directivity of Saturn electrostatic discharges and ionospheric implications. Icarus 61, 508–520.
Zarka, P., Pedersen, B.M., 1983. Statistical study of Saturn electrostatic discharges. J. Geophys. Res. 88, 9007–9018.
Zarka, P. et al., 2006. Physical properties and detection of Saturn's radio lightning. In: Rucker, H.O., Kurth, W.S., Mann, G. (Eds.), Planetary Radio Emissions VI. Austrian Academy of Sciences Press, pp. 111–122.